Hybrid polymer/metal oxide solar cells based on ZnO columnar structures†

Ana M. Peiró,*[a] Punniamoorthy Ravirajan,[bc] Kuveshni Govender,[d] David S. Boyle,[d] Paul O'Brien,[d] Donal D. C. Bradley,[b] Jenny Nelson[b] and James R. Durrant[a]

Received 13th February 2006, Accepted 13th March 2006
First published as an Advance Article on the web 4th April 2006
DOI: 10.1039/b602084d

We focus on the preparation of hybrid polymer/zinc oxide (ZnO) solar cells, in which the metal oxide consists of ZnO columnar structures grown perpendicularly on a flat, dense "backing" layer, as a means to provide a direct and ordered path for photogenerated electrons to the collecting electrode. We used scanning electron microscopy, absorption spectroscopy and photovoltaic device measurements to study the morphology and device performance of the prepared structures. Different solution chemical routes were investigated for the synthesis of the inorganic device components, *i.e.* the ZnO columnar structures and the "backing" layers, which act as a seed-growth layer for the ZnO rods. The growth of the ZnO rods was dependent on the morphological and structural characteristics of the seed layer and moreover, the seed layer itself was also affected by the synthetic conditions for ZnO rod growth. Different polymers (high hole-mobility MEH-PPV based polymer and P3HT) were compared in these structures and power conversion efficiencies of 0.15 and 0.20% were achieved under 1 Sun illumination, respectively. Results are discussed in terms of the optoelectronic properties of the polymers.

Introduction

ZnO has been attracting much attention due to its unique electrical, optoelectronic and luminescent properties that, together with its low cost and ease of preparation, make it potentially useful in a wide range of applications, from nanostructured photonic devices (such as solar cells or light emitting diodes) and piezoelectric devices, to chemical and biological sensors.[1–3]

The application of semiconductor nanostructures within devices is one of the major focuses of contemporary nanotechnology. In particular, the fabrication of well-aligned arrays of elongated ZnO crystallites such as nanorods or nanowires is a subject of increasing interest, as shown by the steady rise in the number of works reported in this area over the last five years. It is well known that microstructure plays a crucial role in many applications, as the properties of the materials depend closely on their crystal size, morphology, aspect ratio and orientation. Ordered ZnO nanostructures are expected to enhance performance of various technologically important devices such as short-wavelength lasers,[4–9] field-emission devices,[10–14] Shottky diodes,[15,16] electroluminescent devices[17,18] and sensors.[19,20] However, most of the work on ZnO nanorod arrays to date has focused on the synthetic methodologies, rather than on their practical applications. Few efforts have been made on the study of the photoelectrochemical performance of ZnO nanorod array films, although zinc oxide has great potential for use as an electrode for dye-sensitized solar cells.[21] Only very recently have a few reports appeared on the use of ZnO nanorods in Gratzel-type solar cells.[22–24] Excitonic solar cells —including Gratzel-type cells, organic and hybrid organic/inorganic solar cells—are promising devices for inexpensive, large-scale solar energy conversion.[22] Hybrid organic/inorganic solar cells are made from composites of conjugated polymers with nanostructured metal oxides, in which the polymer component serves the function of both light absorber and hole conductor, and the metal oxide acts as the electron transporter. External quantum efficiencies of over 40% have been achieved in photovoltaic devices based on conjugated polymers combined with metal oxide nanoparticles or nanoparticle films.[25,26] However, work concerning the application of ZnO nanorod arrays in these structures has been very limited to date.[27,28]

In this study, we present a contribution to the development of hybrid polymer–metal oxide solar cells that incorporate ZnO nanorod arrays as a means to provide a direct and ordered path for photogenerated electrons to the collecting electrode. Fig. 1a shows a schematic of the device structure studied in this work. Basically, the device consists of two electrodes (indium tin oxide-coated glass substrates (ITO) and Au) and an active layer (containing the polymer and the metal oxide), which lies in between. Generated electrons move to the ITO contact through a hole blocking layer ("backing" layer) and holes move to the Au electrode through an electron blocking layer consisting of poly (ethylene dioxythiophene) doped with poly (styrene sulfonic acid) (PEDOT : PSS). Fig. 1b and c show the two active layer designs that have been investigated in this work, namely a backing layer in contact with a polymer film (bi-layer structure) and a columnar

[a]*Centre for Electronic Materials and Devices, Department of Chemistry, Exhibition Road, London, UK SW7 2AZ. E-mail: a.peiro@ic.ac.uk; Fax: +(44) (0)20 7594 5801*
[b]*Centre for Electronic Materials and Devices, Department of Physics, Exhibition Road, London, UK SW7 2AZ*
[c]*Department of Physics, University of Jaffna, Sri Lanka*
[d]*The Manchester Materials Science Centre and Department of Chemistry, Oxford Road, Manchester, UK M13 9PL*
† Electronic supplementary information (ESI) available: device characteristics presented in the order of appearance in the text. See DOI: 10.1039/b602084d

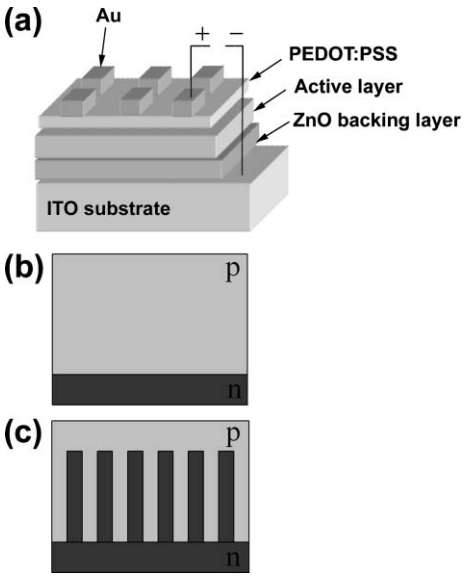

Fig. 1 (a) Schematic of the device structure studied in this work. Active layer designs addressed: (b) backing layer in contact with a polymer film (bi-layer structure) and (c) columnar structure grown on top of a backing layer, where the polymer is interpenetrating the structure.

structure grown on top of a backing layer, with the polymer interpenetrating the structure. In this latter configuration, the backing layer acts as a growth seed for the columnar structure.

Many of the methods reported for the preparation of ZnO nanorod arrays are based on the initial deposition of growth seeds onto the substrate and consequent growth of the ZnO nanorods from these seeds. Catalyst such as Au,[8,29–33] Ag,[34] Co,[14] Cu,[35] or Se[12] have been used as seeds, as well as NiO[36] and GaN.[17] ZnO in the form of nanoparticles[7,9,37–41] or films[13,16,39,42–48] has also been used for this purpose. It has been reported that the use of ZnO growth seeds can lead to better alignment of the ZnO nanorods on the substrate due to the epitactic relationship.[38,49] ZnO films of different thicknesses have been prepared for this purpose through methods such as radiofrequency magnetron sputtering (100 nm,[42] 150 nm,[46] 200 nm,[11] 500 nm[13]), atomic layer deposition,[47] pulsed laser deposition (400 nm,[43] 200 nm[44]), sputter-coating[48] and aqueous solution deposition (500 nm[41]). In this work, the ZnO layer onto which the nanostructures are grown performs the double function of growth seed and hole blocking layer, which prevents direct contact between the polymer and the ITO substrate. This fact implies that this layer needs both to be initially compact and to remain unaltered after the ZnO rod deposition. According to our experience, this is not trivial, as the experimental conditions of crystal growth can lead to dissolution or overetching of the ZnO seed layers, thus decreasing their integrity and compact nature. Importantly, other studies that focus exclusively on synthetic issues have not taken into account the initial compactness of the ZnO seed film and its structure after ZnO rod growth.

The fabrication of working devices is achieved through the optimisation of different cell components such as the ''backing layer'', the ZnO columnar structures and the choice of polymers. In this work, we have investigated different solution chemical routes for the preparation of the inorganic solar cell components (backing layer and columnar structures) onto ITO substrates and we have assessed the performance of a range of conducting polymers. We observe that the structural characteristics of the backing layer have an effect on the growth of the ZnO rods, as well as on the cell performance. Moreover, the synthetic conditions for ZnO rod growth can affect the backing layer through promoting its overetching or dissolution, which in turn also has consequences for the cell performance.

Experimental

A. Materials and methods

Samples were prepared on ITO substrates ($\sim$1 cm^2, 10–15 Ω square^{-1}), which were first cleaned by ultrasonic agitation in acetone and isopropanol and dried under nitrogen flow.

1. Backing layer preparation. Different methods were investigated in order to prepare dense ZnO layers that prevented direct contact of the polymer with the ITO substrate.

1.1. Sol–gel dip-coating method.[50] A solution of zinc acetate dihydrate in n-propanol (120 cm^3) was heated under reflux conditions (130 °C, 20 min). The mixture was allowed to cool to ambient temperature before rapid addition of tetramethylammonium hydroxide (25% in MeOH, 36 cm^3) to yield a transparent nanoparticulate ZnO coating sol, which could be concentrated further by removal of solvent using a rotary evaporator. Different initial concentrations of the ZnO precursor were assayed (0.1–0.5 mol dm^{-3}), in order to obtain films of different thicknesses. Films were prepared by dip-coating the ITO substrates in the sol and sintering in a furnace at 400 °C for 2 min. Heat treatment of the samples at 400 °C for 20 min was also assayed.

1.2. Spin-coating method. Spin-coating methods involved the preparation of 40 nm films through five consecutive deposition processes, using three methods adapted from the literature:[51–53] 1) a 0.6 mol dm^{-3} solution of zinc acetate in dimethylformamide, 2) a 0.20 mol dm^{-3} solution of zinc acetate in methanol, 3) a solution of zinc acetate (0.35 mol dm^{-3}) and monoethanolamine (0.35 mol dm^{-3}) in 2-methoxyethanol. All solutions were left stirring overnight at room temperature before use and subsequently filtered prior to spin-coating at 3000 rpm for 30 s. The as-obtained films were dried at 70 °C for 10 min and calcined at 450 °C for 20 min. Solutions from Method 2 were also spin-coated at different speeds, in order to obtain different thicknesses, ranging from 30 to 70 nm.

1.3. Spray-pyrolysis method. Precursor solutions containing zinc acetate (0.978–1.756 g) in 20 cm^3 of methanol or dimethylformamide were prepared for the spray-pyrolysis method. Deposition took place at 400 °C. After deposition, films were calcined at 400 °C for 20 min, resulting in ZnO films of thickness about 50–70 nm. Best compact layers were obtained with the most concentrated solutions, using methanol as a solvent.

2. ZnO rods preparation. Different methods were investigated in order to prepare ZnO rods onto ZnO backing layers.

2.1. Method 1 (Zn acetate/NH_3/HCHO).[50] Briefly, this method employs an aqueous solution containing zinc acetate (0.025 mol dm^{-3}), formaldehyde (HCHO, 0.016 mol dm^{-3}) and ammonia (NH_3, 0.0083 mol dm^{-3}), at pH 6.9. The substrate was immersed in this solution in an open bath at 90 °C for 2 h.

2.2. Method 2 ($ZnSO_4$/NH_4Cl method).[54] Briefly, an aqueous stock solution of zinc sulfate ($ZnSO_4 \cdot 7H_2O$, 0.02 mol dm^{-3}) and ammonium chloride (NH_4Cl, 0.6 mol dm^{-3}) was prepared. Unless otherwise stated, this solution was further diluted to 0.01 mol dm^{-3} in Zn^{2+} and then, the pH was adjusted to 11.00 with sodium hydroxide (NaOH). Substrates with ZnO dense layers were immersed in 20 cm^3 of this solution and ZnO rod deposition took place at 60 °C for 3–12 h. Following deposition, substrates were rinsed and sonicated in distilled water, and finally dried under nitrogen flow.

2.3. Method 3 (Zn nitrate/HMT).[50] Briefly, this method uses zinc nitrate ($ZnNO_3 \cdot 6H_2O$) as a precursor (0.025 mol dm^{-3}) and hexamethylenetetramine (HMT, 0.025 mol dm^{-3}), at pH 5. The substrate was immersed in this solution in an open bath at 90 °C for 2 h.

3. Polymers. Polymers used were poly(3-hexylthiophene) (P3HT) and poly[(1,4-phenylene-(4-methylphenyl)amino-4,4′-diphenylene-(4-methylphenyl)amino-1,4-phenylene-ethenylene-2-methoxy-5-(2-ethylhexyloxy)-1,4-phenylene-ethenylene)-co-(2,5-dimethoxy-1,4-phenylene-ethenylene-2-methoxy-5-(2-ethylhexyloxy)-1,4-phenylene-ethenylene)] (TPD(4M)-MEH-M3EH-PPV).[26]

4. Device preparation.

4.1. Bi-layer devices. A polymer layer (80 nm) was directly deposited onto the backing layer by spin-coating from a polymer solution in C_6H_5Cl (15–20 mg cm^{-3}) at 2000 rpm. Afterwards, a film of PEDOT : PSS was deposited onto the spin-coated polymer film. Previous studies have demonstrated that device performance of hybrid PPV-based polymer/metal oxide cells is improved by introducing a layer of PEDOT : PSS under the top contact.[55] In this study using P3HT polymer, we have adopted a slightly different procedure, in which isopropanol (1 : 1 or 50% volume) is incorporated into the PEDOT : PSS solution prior to spin coating on the ZnO/P3HT rods devices. The PEDOT : PSS solution was first ultrasonicated for 15 min and then heated at 90 °C for 15 min. The solution was filtered with a 0.45 μm filter and 50% (volume) of isopropanol was then added to the PEDOT : PSS solution. The resulting solution was spin-coated onto the dried polymer layer. Finally, gold top contacts (50 nm) were deposited by evaporation through a shadow mask. Each sample contained six devices of active area ~4.2 mm^2.

4.2. Devices containing ZnO columnar structures. Films were first immersed overnight in a solution of polymer in chlorobenzene (C_6H_5Cl, 2 mg cm^{-3}) or in a 3×10^{-4} mol dm^{-3} solution of amphiphilic polypyridyl ruthenium complex, *cis*-RuLL′(SCN)$_2$ (L = 4,4′-dicarboxylic acid-2,2′-bipyridine, L′ = 4,4′-dinonyl-2,2′-bipyridine) (Z907)[56] in acetonitrile–*tert*-butanol (1 : 1 vol%) at 100 °C. The dip-coated film was then "wiped" by a quick blow with dry nitrogen gas and heated at 50 °C in air. The following steps of the device preparation are identical as those described for bi-layer devices (section 4.1).

B. Electrical measurements

Samples were housed in a home built sample holder with a quartz window for electrical measurements.[55] Current–voltage measurements were obtained using a ScienceTech solar simulator and AM 1.5 spectral filter. Calibration of the light intensity was achieved by using band-pass filters of known transmission combined with a silicon photodiode with independently certified spectral response, calibrated at the ISE Fraunhofer-Institut in Freiburg, Germany. The lamp intensity was adjusted to give close (±10%) agreement with theoretical AM 1.5-equivalent illumination (100 mW cm^{-2}, 1 Sun) over the spectral region of the polymer optical absorption (450–700 nm).

C. Materials characterisation

Scanning electron microscopy (SEM) images were obtained with a Philips XL-30 field emission gun scanning electron microscope. Samples were coated with Au/Pd prior to observation. X-Ray diffraction (XRD) measurements were made on a Philips PW1710 diffractometer with monochromated Cu radiation.

Results and discussion

Optimising the quality of the hole-blocking layer ("backing" layer)

We consider initially the first active layer design, shown in Fig. 1b. In our device structure, a dense layer is needed in order to prevent shunt paths between the polymer and the ITO substrate, and it is referred to as a "hole-blocking" layer or "backing" layer. This layer needs to be compact but, at the same time, thin enough so that the series resistance is kept low. According to our previous studies,[26,57,58] the optimum backing layer thickness for this application is ~50 nm.

Several chemical methods were evaluated for the preparation of backing layers onto ITO, including dip-coating, spin-coating and spray-pyrolysis (see Experimental section for details). Fig. 2 shows SEM images of a selection of the backing layers studied. Fig. 2a shows a film prepared by the dip-coating method. It is obvious from the figure that these films are porous. In order to improve compactness, different concentrations of the ZnO precursor were tested, but our attempts were unsuccessful. ZnO films were also prepared by spin-coating (image not shown) and different ZnO precursors, concentrations and spin velocities were assayed. However, pinholes were present in these films that could be seen with the naked eye, indicating poor film quality. For the spray-pyrolysis (s.-p.) method, different concentrations of the ZnO

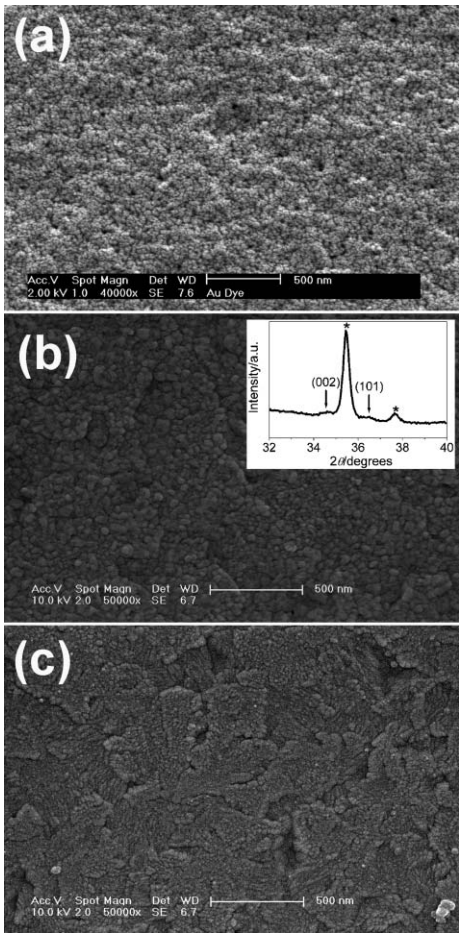

Fig. 2 SEM images of backing layers studied: (a) sol–gel ZnO layer, (b) spray-pyrolysis ZnO layer (from methanolic solution) and (c) spray-pyrolysis TiO_2 layer. Substrate: ITO. Scale bar is 500 nm in all images. Inset in (b) corresponds to the XRD pattern of the ZnO backing layer on ITO substrate. Peak assignments (according to standard diffraction pattern JCPDS 36-1451 of hexagonal phase ZnO) are indicated next to the respective Bragg reflections. The symbol * indicates reflections corresponding to the ITO substrate.

precursor and different solvents were also investigated. Transparent and well-adhered films could only be obtained from zinc acetate solutions in methanol (Fig. 2b) and in DMF (not shown). Finally, Fig. 2c shows a compact TiO_2 backing layer prepared on ITO by the s.-p. method. These TiO_2 layers have already been used and optimised in solid-state dye-sensitised solar cells and hybrid polymer/TiO_2 structures.[55,58,59] The TiO_2 particles in these films are very fine and the morphology of the films closely resembles that of the bare ITO substrate. X-Ray diffraction (XRD) studies were performed on the prepared backing layers, and results corresponding to films (a) and (b) can be found in ref. 50 and in Fig. 2b (inset), respectively. XRD patterns of these films are consistent with the ZnO wurtzite structure. Reflections (002) and (101), corresponding to the s.-p. ZnO backing layer, were detectable but showed very low intensity. This fact is consistent with very thin films comprised of nanometer-sized particles, as revealed in SEM studies (Fig. 2b).

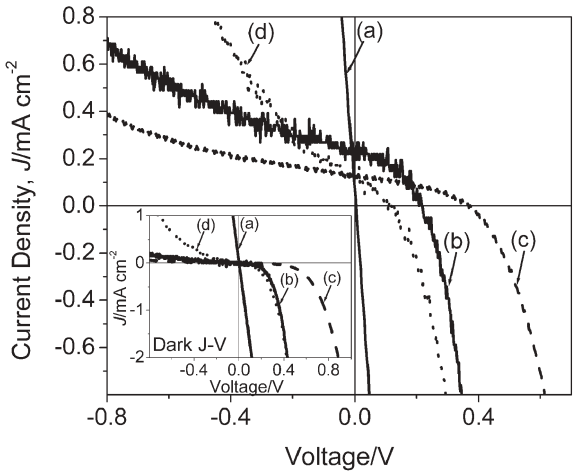

Fig. 3 Current density–voltage (J–V) characteristics of ITO/backing layer/P3HT^{spin}/PEDOT : PSS/Au devices under simulated (100 mW cm^{-2}, AM 1.5) solar illumination and in the dark (inset). ZnO backing layers were prepared by (a) dip-coating and spin-coating, (b) s.-p. from MeOH solution and (c) s.-p. from DMF solution. TiO_2 layers were prepared by the (d) s.-p. method.

Fig. 3 compares the current density–voltage (J–V) characteristics of bi-layer devices based on the above mentioned backing layers and P3HT polymer, under AM 1.5-equivalent illumination (100 mW cm^{-2}, 1 Sun). The inset shows the corresponding dark J–V characteristics of the cells. Devices based on either dip- or spin-coating ZnO backing layers were ''shorted'', which indicates that these layers were not compact enough to prevent contact between the polymer and the ITO substrate. Regarding devices based on s.-p. ZnO layers, best results were obtained for films prepared from methanolic solutions, compared to DMF solutions. The former showed both higher short circuit current density (J_{SC}) and open circuit voltage (V_{OC}), and also better diode behaviour in the dark compared to the latter; this fact being an indication of better compactness in the layers prepared using MeOH as the solvent. Hereafter, reference to s.-p. ZnO backing layers is associated with layers prepared from methanolic solutions. In comparison to devices based on s.-p. TiO_2 dense layers, devices containing s.-p. ZnO layers showed higher J_{SC} but lower V_{OC}. The overall efficiency of these bi-layer devices was $\eta = 0.019\%$ and $\eta = 0.028\%$, for bi-layer devices based on TiO_2 and ZnO, respectively. In the dark, devices based on ZnO showed higher dark current values than TiO_2-based devices. These observations are consistent with the lower conduction band edge of ZnO compared to TiO_2[60] (see ESI† for a detailed summary of the device characteristics of all devices reported in this work).

Growth of ZnO nanorod arrays onto ZnO backing layers.

We now address the second active layer design, as shown in Fig. 2b. For this purpose, ZnO columnar structures were prepared on three selected backing layers: 1) dip-coated porous ZnO layers, 2) s.-p. compact ZnO layers and 3) s.-p. compact TiO_2 layers. The function of these backing layers was binary: i) to act as a hole blocking layer and ii) to act as a seed-growth layer for the ZnO columnar structures.

Several methods are described in the literature for the growth of ZnO nanorods arrays, vapour phase synthesis such as thermal evaporation, chemical vapor deposition and related methods being probably the most extensively employed approaches.[4,5,13,15,17,19,29,31–33,35,36,43,44,61] However, physical methods normally involve complex procedures, sophisticated equipment and high temperatures (in the range of 500 to 900 °C). Alternative methods include electrodeposition,[62] hydrogen treatment of ZnO films,[63] and chemical solution routes such as hydrothermal growth[6,7,11,23,37–39,64–67] and chemical bath deposition.[8,9,41,42,48,50,68] These solution-based routes have become a promising option for large-scale production of microrod and nanorod ZnO arrays on a variety of substrates due primarily to their simplicity and low reaction temperature (60–95 °C).

In this work, synthetic procedures that could be performed in aqueous solvents and at low temperatures were chosen for the growth of the ZnO rod arrays (see Experimental section for details). As an example, Fig. 4 shows the cross-section SEM image of ZnO columnar structures prepared by three different synthetic methods (Methods 1, 2 and 3) on dip-coated porous ZnO layers. The obtained rods possessed aspect ratios of 3.8, 7.3 and 6.7, respectively. X-Ray diffraction (XRD) measurements were recorded for these films (see ref. 50 for films (a) and (c) and Fig. 6c for film (b)) and the obtained diffraction peaks were indexed to the standard diffraction pattern of hexagonal ZnO (JCPDS 36-1451; wurtzite structure) with apparent high crystallinity. Strongly enhanced (002) reflections were observed for all films, consistent with preferential growth of ZnO rods along the *c*-axis (perpendicular to the substrate surface), in agreement with SEM studies.

The current density–voltage (*J–V*) characteristics of devices based on the above mentioned ZnO columnar structures, grown on the three selected backing layers, with PH3T polymer, were studied under AM 1.5-equivalent illumination (100 mW cm^{-2}, 1 Sun) and in the dark. As expected, most of the devices based on ZnO rods grown onto dip-coating ZnO backing layers showed shunting problems due to hole injection through the porous layers to ITO. Regarding devices based on ZnO rods grown onto s.-p. ZnO backing layers, only those involving the growth of the nanorod arrays by Method 2 (6 h) showed acceptable dark current behaviour without large shunt effects (see Fig. 5). All other ZnO rod preparation methods yielded considerably high dark current values, which indicated that the ZnO backing layer may have been damaged during the growth of the ZnO rods. The origin of the problem could be ascribed to partial dissolution or overetching of the ZnO backing layers as a consequence of the higher reaction temperature of 90 °C employed for the growth of the structures by Methods 1 and 3, compared to the growth at 60 °C by Method 2. By comparison, devices based on ZnO nanorod arrays grown on TiO_2 layers showed very poor overall efficiency, which was even lower than that corresponding to devices based on TiO_2 backing layers alone. As an example, devices containing ZnO columnar structures grown by Method 2 (6 h) onto s.-p. TiO_2 backing layers had the following

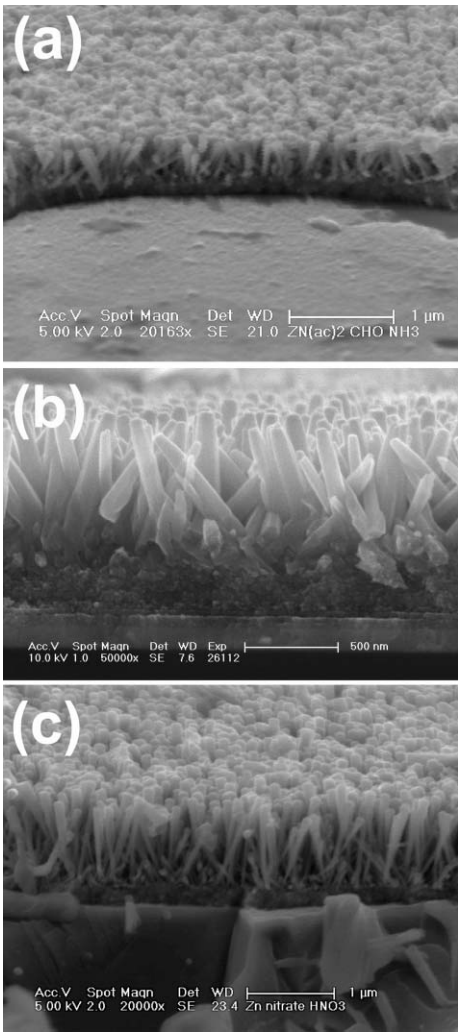

Fig. 4 Cross-section SEM images of ZnO rods grown on dip-coated porous ZnO backing layers by different methods: (a) Method 1, (b) Method 2 (6 h) and (c) Method 3 (see Experimental section). Rods average diameter and length characteristics: (a) 85 nm and 325 nm, (b) 100 nm and 730 nm and (c) 135 nm and 910 nm. Scale bars are 1 μm, 500 nm and 1 μm, respectively.

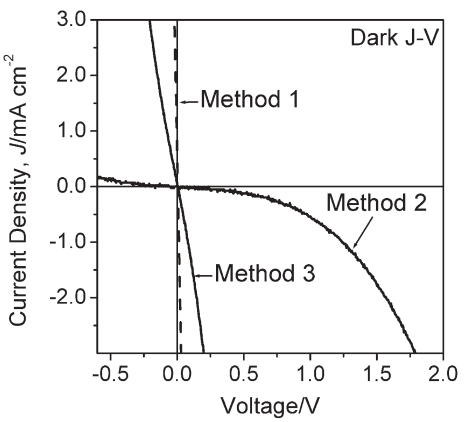

Fig. 5 Dark current density–voltage (*J–V*) characteristics of ITO/s.-p. ZnO backing layer/ZnO rods/P3HT$^{dip+spin}$/PEDOT : PSS/Au devices. Methods 1, 2 (6 h) and 3 were used to prepare the ZnO rod arrays (see Experimental section).

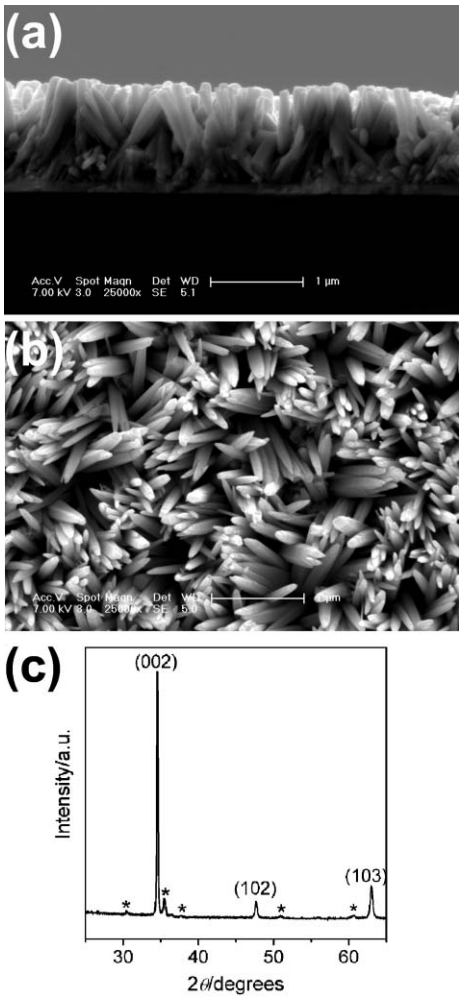

Fig. 6 (a) Cross-section and (b) front view SEM images of ZnO rods grown onto s.-p. ZnO backing layer by Method 2 (6 h). Rod average diameter and length are ~90 nm and ~1 μm, respectively. Scale bar is 1 μm in both images. (c) XRD pattern of the as-synthesised nanorod films. Peak assignments (according to standard diffraction pattern JCPDS 36-1451 of hexagonal phase ZnO) are indicated next to the respective Bragg reflections. The symbol * indicates reflections corresponding to the ITO substrate.

characteristics under 1 Sun: J_{SC} = 0.20 mA cm^{-2}, V_{OC} = 0.06 V, Fill Factor = 28% and η = 0.003%. The poor performance of these devices may be attributed to the energy barrier at the ZnO/TiO_2 interface which hinders electron collection in the ITO contact, as the conduction band energy levels of TiO_2 lie higher than those of ZnO.[60]

SEM characterization of these films showed that the nanorod arrays grown onto TiO_2 backing layers were more densely packed than those grown onto ZnO backing layers and presented inhomogeneity in diameter sizes. Also, regions of aggregates were observed on TiO_2, which increased in size with the time of reaction. These results suggest that the initial deposition of a lattice matched ZnO layer prior to ZnO rod growth critically affects the morphological characteristics of the rods.[40,44,68] Other studies have also shown that the lateral dimensions of the rods appear to be determined by the crystallite size of the seed-growth layer.[40,41,45] In this study, we have observed not only that the growth of the ZnO columnar structures depends on the morphological and structural characteristics of the backing layers, but also that the seed layer itself is affected by the synthetic conditions of rod growth, as revealed by the dark current device characteristics after ZnO rod formation.

As a result of the previous observations, devices consisting of s.-p. ZnO backing layers and ZnO nanorod arrays synthesized by Method 2 were prepared for further study. Fig. 6a and b show cross-section and top view SEM images of the prepared structures respectively. The obtained rods have an aspect ratio of ~11. Fig. 6c shows the corresponding XRD pattern. As mentioned previously, diffraction peaks are readily indexed to the standard diffraction pattern of hexagonal phase ZnO (JCPDS card No. 36-1451) and the presence of a strongly enhanced (002) peak is consistent with preferential growth of wurtzite ZnO rods along the *c*-axis.

Our aim was to modify some of the reaction parameters of Method 2, such as reaction time and reagents concentration, in order to assess their effect on the rod morphology and, consequently, on device performance. Firstly, we evaluated the effect of the reaction time. ZnO rod growth was performed for different time periods, ranging from 3 to 24 h. Fig. 7 (a,b) and (c,d) show SEM images of the ZnO nanorod arrays obtained on s.-p. ZnO backing layers after 3 h and 12 h of reaction respectively. Apparently, the dimensions of the rods are not greatly influenced by reaction time in the time interval chosen. The most likely explanation for the observation is a critical drop in supersaturation through consumption of ZnO precursor during the initial 3 h of reaction, as the rod lengths were similar for the 3 h to 12 h reaction periods (see Fig. 7a, 6a and 7c for reaction times of 3 h, 6 h and 12 h, respectively). However, both the length and diameter of the rods appeared to be more homogeneous for longer reaction times (~1.25 μm and ~70 nm, respectively, for 12 h reaction, compared to 0.95–1.25 μm and 95–110 nm for 3 h reaction) with aspect ratios for these structures of ~11 (12 h) and ~17 (3 h). On the other hand, at long reaction times, such as 12 h or longer, deposition of star-like crystals took place onto the ZnO nanorod arrays (see Fig. 7e and f). These twinned crystalline ZnO structures presumably formed by homogeneous nucleation in solution rather than by heterogeneous nucleation.[50] Although most of these deposits could be easily removed from the ZnO rod film surface by ultrasonication, some of them remained deeply inserted into the ZnO rod films; their presence obviously undesirable in terms of optimising cell performance. Devices based on structures grown for short reaction times showed better overall performance (similar results were obtained for 3 to 6 h) than for longer reaction times (12 to 24 h). This is due partly to the absence of star-like deposits in the former and relatively increased ZnO rod aspect ratio. Best device characteristics for ITO/s.-p. ZnO backing layer/ZnO rods$^{\text{Method 2(6h)}}$/P3HT$^{\text{dip+spin}}$/PEDOT : PSS/Au structures were: J_{SC} = 1.33 mA cm^{-2}, V_{OC} = 0.15 V, Fill Factor = 30.9% and η = 0.062%.

Secondly, we studied the effect of different concentrations (0.001–0.01 mol dm^{-3}) of ZnO precursor on the dimensions of the ZnO nanorod arrays. SEM images of the films showed that lower concentration of precursor produced smaller rods

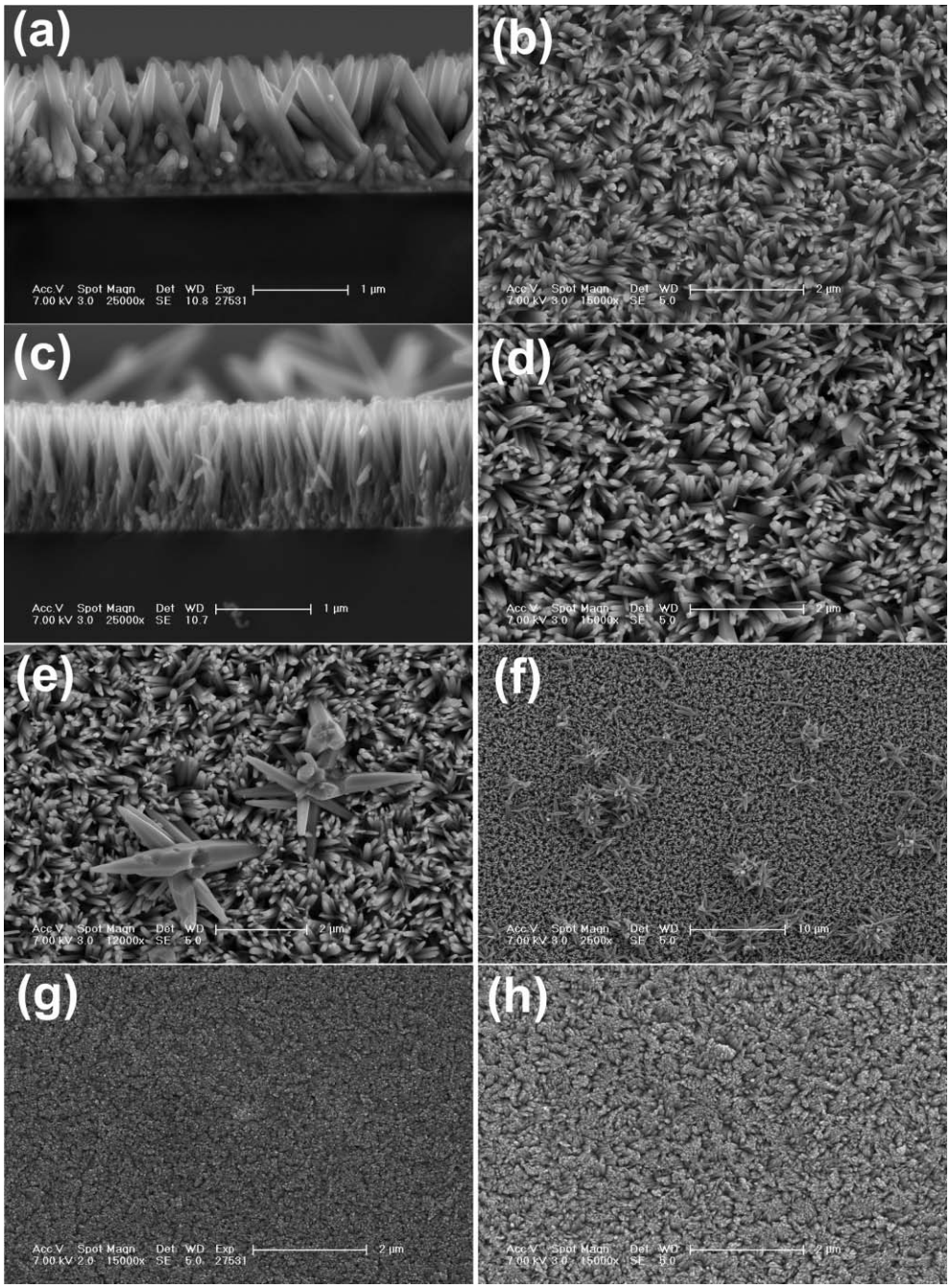

Fig. 7 Cross-section and front view SEM images of ZnO rods grown onto s.-p. ZnO dense layer by Method 2 for (a, b) 3 h and (c, d) 12 h. Concentration of Zn^{2+} precursor: 0.01 mol dm^{-3}. Diameter and length of rods are (a, b) 110 nm and 0.94–1.25 μm and (c, d) 72 nm and 1.25 μm, respectively. (e, f) SEM images of selected area in ZnO rod film (12 h), in which star-like ZnO particles are found. (g, h) SEM image of ZnO rods grown onto s.-p. ZnO layers by Method 2 (3 h), using 0.001 and 0.005 mol dm^{-3} Zn^{2+} precursor solutions, respectively. Scale bars are (a) 1 μm, (b) 2 μm, (c) 1 μm, (d, e) 2 μm, (f) 10 μm and (g, h) 2 μm.

(compare Zn^{2+} concentrations 1, 5 and 10 × 10^{-3} mol dm^{-3} in Fig. 7g, h and b, respectively). The fact that smaller rods are produced by decreasing the concentration of Zn^{2+}, while maintaining those of other reagents, has been reported by others.[38] The same effect has been observed by decreasing the overall concentration of the reagents.[48,65] However, images of the nanorods arrays were not shown in those studies. We are aware that these smaller rods may be more suitable for metal oxide/polymer solar cells, as their dimensions are in the same range as the polymer exciton diffusion length.[40] For this reason, work is in progress to assess the performance of these structures in hybrid solar cell devices. In this paper however, we focus on the optimisation of device structures containing ZnO rods prepared by Method 2, using an initial concentration of Zn^{2+} of 0.01 mol dm^{-3}, which corresponds to structures with larger dimensions (as seen in Fig. 7a and b).

Optimisation of devices based on the developed active layer structures.

Finally, we discuss the optimisation of devices based on the developed active layer structures containing ZnO rods prepared by Method 2. In previous studies,[27] we found that charge recombination in the active layer structure containing vertically aligned ZnO nanorods treated with an amphiphilic dye (Z907 dye) prior to P3HT polymer deposition is remarkably slow, with a half life of $\sim$6 ms. We also observed that the incorporation of a layer of the amphiphilic dye (Z907 dye) onto the ZnO rod structures, prior to the P3HT polymer deposition, was favourable for the device performance. The Z907 dye layer is regarded as an interfacial modifier, which improves the wetting of the oxide surface by the polymer. Moreover, the energy level structure at the ZnO/Z907^{dip}/P3HT^{spin} interface seems to enable electron cascade from P3HT to ZnO whilst blocking hole transfer, thus improving charge separation at the ZnO interface. A detailed study of the mechanism of these processes is described in ref. 27. Here we extend this approach to another polymer, namely TPD(4M)-MEH-M3EH-PPV, and we incorporate an additional dip-coating step for the polymer prior to spin-coating. In our previous study on hybrid polymer/TiO_2 solar cells,[58] TPD(4M)-MEH-M3EH-PPV polymer led to the best performance from among a group of similar polymers, due to its specific combination of desirable properties. Our device configuration is ITO/s.-p. ZnO backing layer/ZnO rods^{Method2}/Z907^{dip}/Polymer$^{dip+spin}$/PEDOT : PSS/Au. We note that the incorporation of the additional dip-coating step does not modify the overall cell performance. Fig. 8a shows the current density–voltage characteristics of devices based on ZnO nanorod arrays grown by Method 2 on s.-p. ZnO backing layers and the above mentioned hole conducting polymers, in the presence of a Z907 dye as an interface modifier layer. Measurements were performed under AM 1.5-equivalent illumination (100 mW cm^{-2}, 1 Sun) and in the dark (see inset). All these devices showed good rectification properties in the dark. Under 1 Sun illumination, best results were obtained with P3HT polymer (J_{SC} = 1.73 mA cm^{-2}, V_{OC} = 0.30 V, Fill Factor = 38.9 and η = 0.20%). Devices using TPD(4M)-MEH-M3EH-PPV polymer showed an overall efficiency of 0.15.%. Fig. 8b shows the UV-vis optical absorption spectra of the active layers containing the ZnO nanorod structures and the respective polymers. The absorption maximum for TPD(4M)-MEH-M3EH-PPV and P3HT is 439 nm and 550 nm, respectively, and the time of flight hole mobilities for both polymers are $\sim 10^{-4}$ cm^2 V^{-1} s^{-1} at 2.5 $\times$ 10^5 V cm^{-1}.[26,69] Although the absorption of TPD(4M)-MEH-M3EH-PPV polymer is relatively blue-shifted compared to P3HT, both devices showed comparable performance. This is probably due to the higher exciton diffusion length of TPD(4M)-MEH-M3EH-PPV polymer (15 $\pm$ 4 nm) compared to P3HT polymer ($\sim$5 nm).[58,70]

Conclusions

We have studied the use of ZnO nanorod arrays in hybrid polymer/metal oxide solar cells. Different solution chemical routes have been investigated for the preparation of the inorganic device components, such as the ''backing layers'' and the ZnO columnar structures. We have observed that the growth of the ZnO nanorod arrays is dependent on the morphological and structural characteristics of the seed layer, but also that the seed layer itself is affected by the synthetic conditions of rod growth. This fact has consequences on the cell performance. Two polymers (TPD(4M)-MEH-M3EH-PPV and P3HT) have been essayed in hybrid solar cells based on the ZnO nanorod arrays and best results have been obtained using a molecular interfacial modifier and P3HT polymer as hole conductor (J_{SC} = 1.73 mA cm^{-2}, V_{OC} = 0.30 V, Fill Factor = 38.9% and η = 0.20%). Further work is in progress in order to assess the cell performance of the smaller nanorod structures prepared in this work.

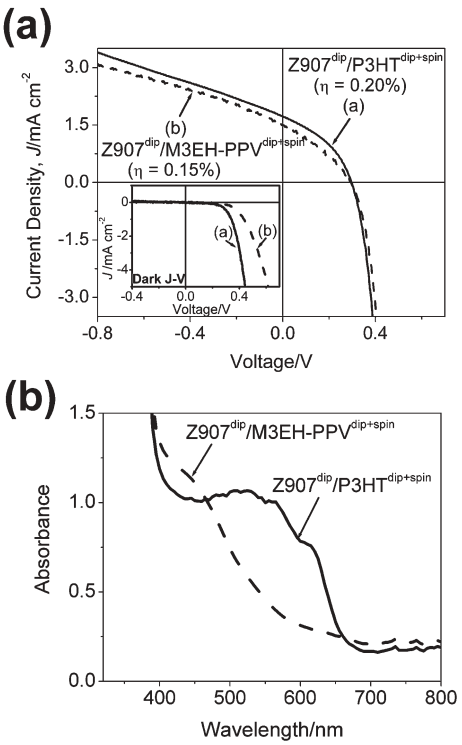

Fig. 8 a) Current density–voltage (J–V) characteristics of ITO/s.-p. ZnO backing layer/ZnO rods^{Method2}/Z907^{dip}/polymer$^{dip+spin}$/PEDOT : PSS/Au devices under simulated (100 mW cm^{-2}, AM 1.5) solar illumination and in the dark (inset). Polymers: TPD(4M)-MEH-M3EH-PPV and P3HT. (b) UV-vis spectra of structures in (a), before deposition of the PEDOT : PSS/Au layers.

Acknowledgements

We are grateful to Professor H. H. Hörhold and Merck Chemicals Ltd for providing the TPD(4M)-MEH-M3EHPPV and P3HT polymers used in this study. We thank M. K. Nazeeruddin and M. Grätzel from the Laboratory for Photonics and Interfaces, Switzerland, for supplying Z907 dye. We acknowledge EPSRC and the Commission of the European Community (Project MOLYCELL Contract No. 502783) for their financial assistance. Ana M. Peiró acknowledges the Spanish Secretaría de Estado de Universidades e Investigación del Ministerio de Educación y Ciencia for a postdoctoral fellowship.

References

1 Y. Wu, H. Yan, M. Huang, B. Messer, J. H. Song and P. Yang, *Chem. Eur. J.*, 2002, **8**, 1260.
2 G. Yi, C. Wang and W. Il Park, *Semicond. Sci. Technol.*, 2005, **20**, S22.
3 Y. W. Heo, D. P. Norton, L. C. Tien, Y. Kwon, B. S. Kang, F. Ren, S. J. Pearton and J. R. LaRoche, *Mater. Sci. Eng. R*, 2004, **47**, 1.
4 M. H. Huang, S. Mao, H. Feick, H. Yan, Y. Wu, H. Kind, E. Weber, R. Russo and P. Yang, *Science*, 2001, **292**, 1897.
5 P. Yang, H. Yan, S. Mao, R. Russo, J. Johnson, R. Saykally, N. Morris, J. Pham, R. He and H.-J. Choi, *Adv. Funct. Mater.*, 2002, **12**, 323.
6 A. L. Pan, R. B. Liu, S. Q. Wang, Z. Y. Wu, L. Cao, S. S. Xie and B. S. Zou, *J. Cryst. Growth*, 2005, **282**, 125.
7 J.-H. Choy, E.-S. Jang, J. H. Won, J.-H. Chung, D.-J. Jang and Y.-W. Kim, *Adv. Mater.*, 2003, **15**, 1911.
8 K. Govender, D. S. Boyle, P. O'Brien, D. Brinks, D. West and D. Coleman, *Adv. Mater.*, 2002, **14**, 1221.
9 L. E. Greene, M. Law, J. Goldberger, F. Kim, J. C. Johnson, Y. Zhang, R. J. Saykally and P. Yang, *Angew. Chem., Int. Ed.*, 2003, **42**, 3031.
10 Y. W. Zhu, H. Z. Zhang, X. C. Sun, S. Q. Feng, J. Xu, Q. Zhao, B. Xiang, R. M. Wang and D. P. Yu, *Appl. Phys. Lett.*, 2003, **83**, 144.
11 C.-H. Hung and W.-T. Whang, *J. Cryst. Growth*, 2004, **268**, 242.
12 H. Z. Zhang, R. M. Wang and Y. W. Zhu, *J. Appl. Phys.*, 2004, **96**, 624.
13 Y.-K. Tseng, C.-J. Huang, H.-M. Cheng, I.-N. Lin, K.-S. Liu and I.-C. Chen, *Adv. Funct. Mater.*, 2003, **13**, 811.
14 C. J. Lee, T. J. Lee, S. C. Lyu, Y. Zhang, H. Ruh and H. J. Lee, *Appl. Phys. Lett.*, 2002, **81**, 3648.
15 W. I. Park, G. C. Yi, M. Kim and S. J. Pennycook, *Adv. Mater.*, 2002, **14**, 1841.
16 W. I. Park, G.-C. Yi, J.-W. Kim and S.-M. Park, *Appl. Phys. Lett.*, 2003, **82**, 4358.
17 W. I. Park and G. C. Yi, *Adv. Mater.*, 2004, **16**, 87.
18 S. W. Kim, T. Kotani, M. Ueda and S. Fujita, *Appl. Phys. Lett.*, 2003, **83**, 3593.
19 M.-C. Jeong, B.-Y. Oh, W. Lee and J.-M. Myoung, *Appl. Phys. Lett.*, 2005, **86**, 103105.
20 G. S. Trivikrama Rao and D. Tarakarama Rao, *Sens. Actuators B: Chem.*, 1999, **55**, 166.
21 N. Beermann, L. Vayssieres, S.-E. Lindquist and A. Hagfeldt, *J. Electrochem. Soc.*, 2000, **147**, 2456.
22 M. Law, L. E. Greene, J. C. Johnson, R. Saykally and P. Yang, *Nat. Mater.*, 2005, **4**, 455.
23 M. Guo, P. Diao and S. Cai, *Appl. Surf. Sci.*, 2005, **249**, 71.
24 J. B. Baxter and E. S. Aydil, *Appl. Phys. Lett.*, 2005, **86**, 053114.
25 W. J. E. Beek, M. M. Wienk and R. A. J. Janssen, *Adv. Mater.*, 2004, **16**, 1009.
26 P. Ravirajan, S. A. Haque, J. R. Durrant, H. J. P. Smit, J. M. Kroon, D. D. C. Bradley and J. Nelson, *Appl. Phys. Lett.*, 2005, **86**, 143101.
27 P. Ravirajan, A. M. Peiró, M. K. Nazeeruddin, M. Graetzel, J. R. Durrant and J. Nelson, *J. Phys. Chem. B*, in press.
28 D. C. Olson, J. Piris, R. T. Collins, S. E. Shaheen and D. S. Ginley, *Thin Solid Films*, 2006, **496**, 26–29.
29 N. Pan, X. Wang, K. Zhang, H. Hu, B. Xu, F. Li and J. G. Hou, *Nanotechnology*, 2005, **16**, 1069.
30 H. J. Fan, B. Fuhrmann, R. Scholz, F. Syrowatka, A. Dadgar, A. Krost and M. Zacharias, *J. Cryst. Growth*, 2006, **287**, 34.
31 H. J. Fan, W. Lee, R. Scholz, A. Dadgar, A. Krost, K. Nielsch and M. Zacharias, *Nanotechnology*, 2005, **16**, 913.
32 X. Q. Meng, D. Z. Shen, J. Y. Zhang, D. X. Zhao, Y. M. Lu, L. Dong, Z. Z. Zhanga, Y. C. Liu and X. W. Fan, *Solid State Commun.*, 2005, **135**, 179.
33 H. Chik, J. Liang, S. G. Cloutier, N. Kouklin and J. M. Xu, *Appl. Phys. Lett.*, 2004, **84**, 3376.
34 J. W. P. Hsu, Z. R. Tian, N. C. Simmons, C. M. Matzke, J. A. Voigt and J. Liu, *Nano Lett.*, 2005, **5**, 83.
35 S. Y. Li, C. Y. Lee and T. Y. Tseng, *J. Cryst. Growth*, 2003, **247**, 357.
36 S. C. Lyu, Y. Zhang, H. Ruh, H. J. Lee, H. WookShim, E. K. Suh and C. J. Lee, *Chem. Phys. Lett.*, 2002, **363**, 134.
37 Z. R. Tian, J. Z. Voigt, J. Liu, B. Mckenzie, M. J. Mcdermott, M. A. Rodriguez and H. Xu, *Nat. Mater.*, 2003, **2**, 821.
38 M. Guo, P. Diao and S. Cai, *J. Solid State Chem.*, 2005, **178**, 1864.
39 J. H. Lee, I. C. Leu and M. H. Hon, *J. Cryst. Growth*, 2005, **275**, e2069.
40 L. E. Greene, M. Law, D. H. Tan, M. Montano, J. Goldberger, G. Somorjai and P. Yang, *Nano Lett.*, 2005, **5**, 1231.
41 D. S. Boyle, K. Govender and P. O'Brien, *Chem. Commun.*, 2002, 80.
42 C.-C. Lin, H.-P. Chen, H.-C. Liao and S.-Y. Chen, *Appl. Phys. Lett.*, 2005, **86**, 183103.
43 X. Zhang, L. Wang and G. Zhou, *Rev. Adv. Mater. Sci.*, 2005, **10**, 69.
44 J. Jie, G. Wang, Y. Chen, X. Han, Q. Wang, B. Xu and J. G. Hou, *Appl. Phys. Lett.*, 2005, **86**, 031909.
45 H. Zhang, D. Yang, X. Ma and D. Que, *J. Phys. Chem. B*, 2005, **109**, 17055.
46 H. Yu, Z. Zhang, M. Han, X. Hao and F. Zhu, *J. Am. Chem. Soc.*, 2005, **127**, 2378.
47 Q. Li, V. Kumar, Y. Li, H. Zhang, T. J. Marks and R. P. H. Chang, *Chem. Mater.*, 2005, **17**, 1001.
48 R. B. Peterson, L. F. Clark and A. G. Brian, *Langmuir*, 2004, **20**, 5114.
49 Z. L. Wang, *Mater. Today*, 2004, **7**, 26.
50 K. Govender, D. S. Boyle, P. B. Kenway and P. O'Brien, *J. Mater. Chem.*, 2004, **14**, 2575.
51 N. R. S. Farley, C. R. Staddon, L. Zhao, K. W. Edmonds, B. L. Gallagher and D. H. Gregory, *J. Mater. Chem.*, 2004, **14**, 1087.
52 Y. Natsume and H. Sakata, *Thin Solid Films*, 2000, **372**, 30.
53 J. H. Lee, K. H. Ko and B. O. Park, *J. Cryst. Growth*, 2003, **247**, 119.
54 S. Yamabi and H. Imai, *J. Mater. Chem.*, 2002, **12**, 3773.
55 P. Ravirajan, S. A. Haque, J. R. Durrant, D. Poplavskyy, D. D. C. Bradley and J. Nelson, *J. Appl. Phys.*, 2004, **95**, 1473.
56 P. Wang, S. M. Zakeeruddin, I. Exnar and M. Grätzel, *Chem. Commun.*, 2002, 2972.
57 P. Ravirajan, S. A. Haque, D. Poplavskyy, J. R. Durrant, D. D. C. Bradley and J. Nelson, *Thin Solid Films*, 2004, **451–452**, 624.
58 P. Ravirajan, S. A. Haque, J. R. Durrant, D. D. C. Bradley and J. Nelson, *Adv. Funct. Mater.*, 2005, **15**, 609.
59 U. Bach, D. Lupo, P. Comte, J. E. Moser, F. Weissörtel, J. Salbeck, H. Spreitzer and M. Grätzel, *Nature*, 1998, **395**, 583; L. Kavan and M. Grätzel, *Electrochim. Acta*, 1995, **40**, 643.
60 Y. Xu and M. A. A. Shoonen, *Am. Mineral.*, 2000, **85**, 543.
61 B. P. Zhang, N. T. Binh, Y. Segawa, K. Wakatsuki and N. Usami, *Appl. Phys. Lett.*, 2003, **83**, 1635; X. Q. Meng, D. X. Zhao, J. Y. Zhang, D. Z. Shen, Y. M. Lu, Y. C. Liu and X. W. Fan, *Chem. Phys. Lett.*, 2005, **407**, 91; S. C. Lyu, Y. Zhang, C. J. Lee, H. Ruh and H. J. Lee, *Chem. Mater.*, 2003, **15**, 3294; L. Wang, X. Zhang, S. Zhao, G. Zhou, Y. Zhou and J. Qi, *Appl. Phys. Lett.*, 2005, **86**, 024108; C. Geng, Y. Jiang, Y. Yao, X. Meng, J. A. Zapien, C. S. Lee, Y. Lifshitz and S. T. Lee, *Adv. Funct. Mater.*, 2004, **14**, 589; Y. Wu, H. Yan and P. Yang, *Top. Catal.*, 2002, **19**, 197; H. Z. Zhang, X. C. Sun, R. M. Wang and D. P. Yu, *J. Cryst. Growth*, 2004, **269**, 464; Y. Xu X, H. Z. Zhang, Q. Zhao, Y. F. Chen, J. Xu and D. P. Yu, *J. Phys. Chem. B*, 2005, **109**, 1699; Y. Zhang, L. Wang, X. Liu, Y. Yan, C. Chen and J. Zhu, *J. Phys. Chem. B*, 2005, **109**, 13091; S. C. Liu and J. J. Wu, *J. Mater. Chem.*, 2002, **10**, 3125.
62 L. Xu, Y. Guo, Q. Liao, J. Zhang and D. Xu, *J. Phys. Chem. B*, 2005, **109**, 13519; R. Konenkamp, K. Boedecker, M. C. Lux-Steiner, M. Poschenrieder, F. Zenia, C. L. Clement and S. Wagner, *Appl. Phys. Lett.*, 2000, **77**, 2575.
63 J. Wu, H. Wen, C. Tseng and S. Liu, *Adv. Funct. Mater.*, 2004, **14**, 806.
64 Z. K. Tang, G. K. L. Wong, P. Yu, M. Kawasaki, A. Ohtomo, H. Koinuma and Y. Segawa, *Appl. Phys. Lett.*, 1998, **72**, 3270.
65 L. Vayssieres, *Adv. Mater.*, 2003, **15**, 464.
66 L. Vayssieres, K. Keis, A. Hagfeldt and S.-E. Lindquist, *Chem. Mater.*, 2001, **13**, 4395.
67 Z. Wang, X.-f. Qian, J. Yin and Z.-k. Zhu, *Langmuir*, 2004, **20**, 3441.
68 Y. Tak and K. Yong, *J. Phys. Chem. B*, 2005, **109**, 19263.
69 S. A. Choulis, Y. Kim, J. Nelson, D. D. C. Bradley, M. Giles, M. Shkunov and I. McCulloch, unpublished work.
70 M. Theander, A. Yartsev, D. Zigmantas, V. Sundstrom, W. Mammo, M. R. Anderson and O. Inganas, *Phys. Rev. B*, 2000, **61**, 12957.

